Progress in Organic Coatings 180 (2023) 107544

Contents lists available at ScienceDirect

Progress in Organic Coatings

journal homepage: www.elsevier.com/locate/porgcoat

Evaluation of epoxy-based coating degradation under thermal insulation at elevated temperatures on different steel substrates

Qing Cao [a], Ibukun Oluwoye [a], Thunyaluk Pojtanabuntoeng [a,*], Hanan Farhat [b], Mariano Iannuzzi [a]

[a] Curtin Corrosion Centre, Curtin University, WA 6102, Australia
[b] Corrosion Centre, Qatar Environment and Energy Research Institute, Hamad Bin Khalifa University, Qatar

ARTICLE INFO

Keywords:
Corrosion under insulation
Coating
Coating degradation

ABSTRACT

Corrosion under insulation (CUI) remains one of the most critical issues in the petrochemical industry. In a typical CUI system, protective coatings (organic or metallic) are used primarily as the last barrier to prevent the rapid corrosion of the metallic substrate. However, organic coatings exposed to high operating temperatures and thermal cycling conditions are susceptible to failure and thus require coating performance evaluations under representative thermal insulation conditions. This study presents experimental designs to investigate the degradation of an organic polyamine-cured epoxy coating under accelerated laboratory test conditions. Additionally, a systematic CUI evaluation protocol for high-temperature organic coating performance is presented. The method involved specially designed apparatus to simulate CUI systems and characterisation techniques, such as visual inspection, adhesion test, peel-off test, scanning electron microscopy, electrochemical impedance spectroscopy, and chemical analysis using Fourier-transform infrared spectroscopy, and differential scanning calorimetry. The results showed that polyamine-based epoxy coating experienced thermal degradation starting at temperatures above 130 °C under mineral wool insulation in accelerated and cyclic CUI tests. Chemical degradation was the primary mode of degradation, with the formation of carbonyl functional groups and increased glass transition temperature observed at higher exposure temperatures. The proposed combination of electrochemical, spectroscopic, mechanical, and microscopy techniques allows quantifying coating performance under insulation and subsequently provides insights into predicting coatings' service lifetime.

1. Introduction

Corrosion under insulation (CUI) is one of the most detrimental issues in the petrochemical and process industries, drawing much attention from operators and engineers due to the associated high maintenance costs. The problem, if left unattended, inevitably creates undesirable and detrimental consequences, e.g., piping rupture and liquid/gas leakages [1–3]. By employing barrier protection on the metallic substrate, the underlying metal can be prevented from early premature failure caused by external corrosive agents, such as water (e.g., from rainfall and moisture condensation), oxygen, and corrosive contaminants. Epoxy-based coatings are conventionally used for protection against CUI due to their superior mechanical and chemical properties that determine the extended overall lifespan of a coating, providing reliable and protective layers for corrosion mitigation [4,5]. Moreover, epoxy-based coatings with an amine curing agent are one of the most often used coatings to achieve desirable cross-linking, chemical, mechanical, and thermal properties [6,7]. It is crucial to investigate the performance of epoxy coatings at elevated temperatures, close to their operating limits and the upper CUI range (e.g., 150–175 °C). The first complication is that infiltrated water and moisture tends to be retained within the annular space between insulation and coated substrate. Additionally, water evaporation is limited by the presence of insulation and cladding, prolonging 'immersion' time and consequently leading to a scenario favourable to corrosion initiation and propagation.

There is no consensus on the most suitable international standard for coating performance evaluation under insulation. ISO 19277 [8] is the only published industrial guideline on CUI coating evaluation. In this standard, the assessment requires simple characterisation such as pull off adhesion and visual observation. In insulated piping equipment, the criteria for selecting appropriate coating materials vary depending on service temperature (both maximum temperature and during

* Corresponding author.
E-mail address: Thunyaluk.pojtanabuntoeng@curtin.edu.au (T. Pojtanabuntoeng).

https://doi.org/10.1016/j.porgcoat.2023.107544
Received 14 December 2022; Received in revised form 16 February 2023; Accepted 8 March 2023
Available online 31 March 2023
0300-9440/© 2023 Elsevier B.V. All rights reserved.

Table 1
Nominal chemical compositions of carbon and stainless steel substrates.

Chemical component	Fe %	C max.%	Mn %	P max.%	S max.%	Si min.%	Cr max.%	Cu max.%	Mo max.%	Ni max.%	V max.%
A106 CS	~97	0.30	0.29–1.06	0.035	0.035	0.10	0.40	0.40	0.15	0.40	0.08
316L SS	~76	0.03	2.00	0.045	0.03	1.00	16.00–18.00	–	2.00–3.00	–	–

Table 2
DFT measurement of coatings applied on carbon steel (A106 grade B) and stainless steel (316L SS) substrates.

DFT measurements (μm)	#1	#2	#3	#4	#5	#6	#7	#8	#9	#10	Average ± SD
A106 CS	492	502	503	548	563	516	483	515	502	498	512 ± 24
316L SS	756	891	731	725	713	751	652	705	640	658	722 ± 68

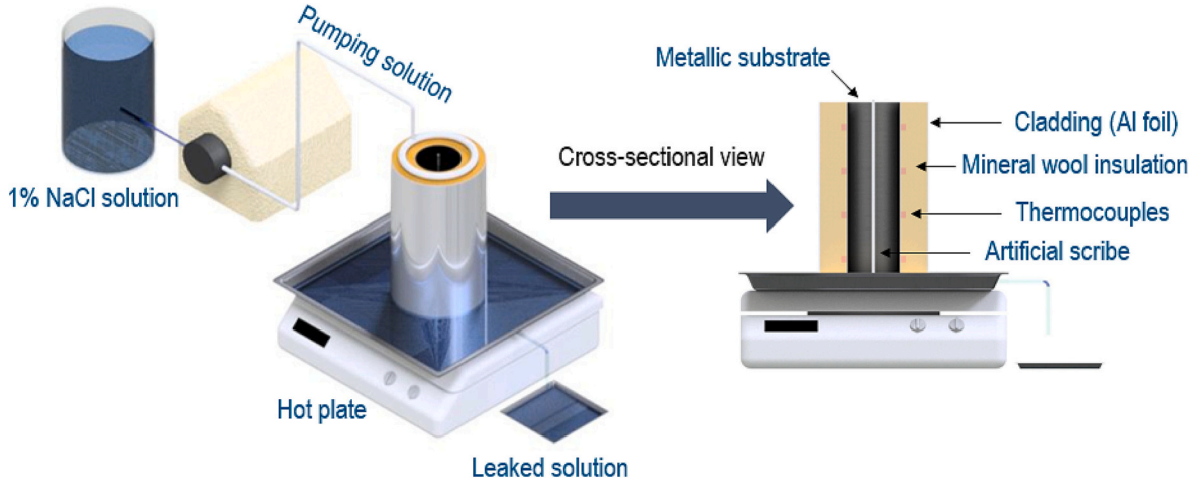

Fig. 1. Schematics (front and cross-sectional views) of vertical pipe setup to investigate coating degradation under thermal insulation at elevated temperatures.

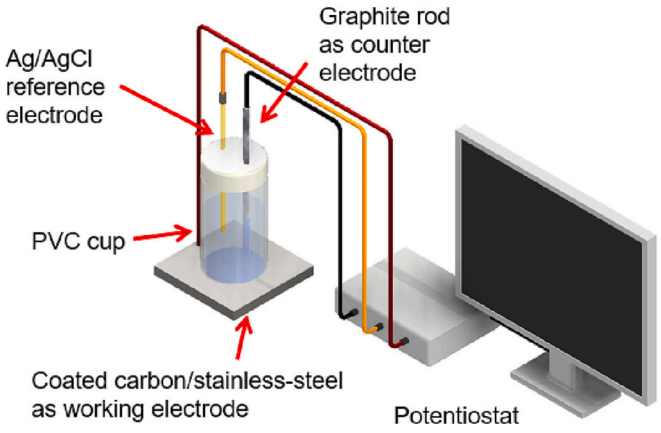

Fig. 2. Schematic of customised three-electrode cell for electrochemical impedance spectroscopy characterisation, with all electrodes submerged in 3.5 wt% NaCl solution.

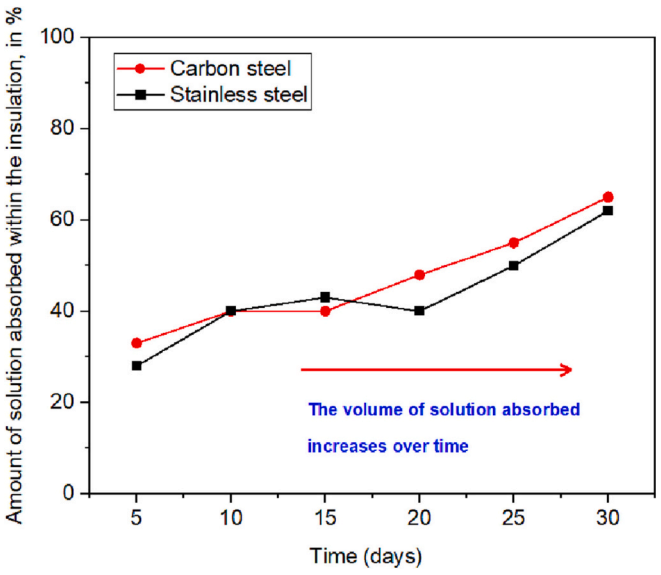

Fig. 3. The amount of solution intake within the insulation, in %, as a function of exposure time, from day 5 to day 30. An increasing amount of absorbed solution was observed as the thermal exposure period increased.

downtime), requirement for surface preparation, required dry film thickness [9]. Indeed, life cycle cost analysis may be performed to aid the selection of coatings where maintenance intervals and cost of coatings and application on site are considered [10]. The underlying causes for coating degradation under elevated temperatures can be complex, and the coating morphologies may experience different degrees of changes that are intercorrelated with changes in the coating property and performance. By using complementary characterisation and analytical methodologies, coating behaviour can be fully examined and understood. Therefore, one of the core objectives of this study was to implement a methodology to investigate coating performance under thermal insulation systematically.

Epoxy thermoset coatings comprise the resin, curing agent (e.g.,

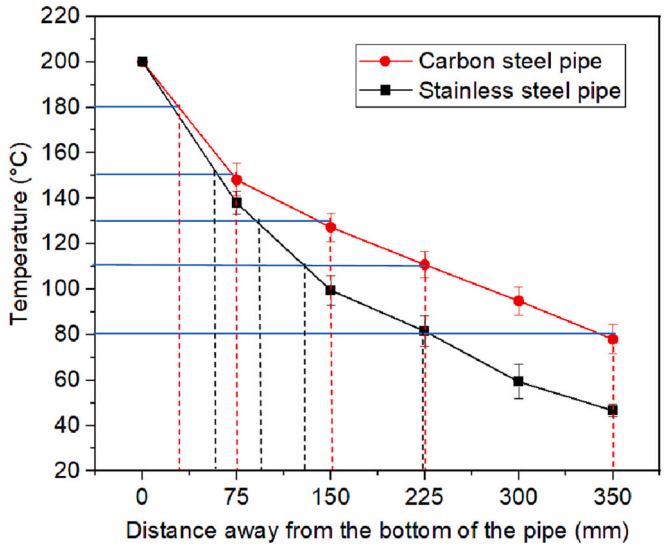

Fig. 4. Coating surface temperature profile measured on coated carbon steel (red line) and coated stainless steel (black line) vertical pipes. The blue lines represent the desired temperatures of interest for further analysis. (For interpretation of the references to color in this figure legend, the reader is referred to the web version of this article.)

polyamine, etc.), and other components such as plasticiser, preservative, and chain-terminating compound. Zargarnezhad et al. reviewed the mass transport of H_2O in epoxy coatings and provided insights on probabilistic models to relate the likelihood of failures based on the declining properties of the coatings [11]. In a CUI scenario, the structure of epoxy thermoset coatings is prone to deterioration by hydrolysis (due to the presence of moisture) and thermal degradation. The thermal degradation pathway can affect the resin and the curing agent, leading to depolymerisation and the formation of low molecular weight species [12,13]. Hydrolysis, on the other hand, depends on the hydrophilic groups, mainly secondary hydroxyl and amide ends. The degradation stimuli can result in substantial changes in the mechanical properties of the coating. Epoxy coatings exposed at high temperatures tend to have increased brittleness, while heat and oxygen enhance the thermo-oxidation process of epoxy coating materials during a hygrothermal aging process [14,15].

In this paper, a modified vertical pipe was set up to study coating performance on carbon and stainless-steel substrates under insulation in a thermal cyclic test setting. Evaluation techniques included visual examination (identifying rusting, cracking, blistering, and discolouration), pull-off adhesion and peel-off tests, chemical and thermal analysis using Fourier-transform infrared spectroscopy (FTIR) and differential scanning calorimetry (DSC), electrochemical measurements to study coating barrier properties as a function of thermal exposure. Insight into coating degradation was further discussed using the broad range of characterisation techniques. Observations were compared with non-exposed baseline samples.

2. Experimental

2.1. Materials

A commercial coating formulated from Bisphenol-A/F epoxy resin and polymeric cycloaliphatic amines as primary components with a maximum recommended service temperature of 150 °C was used in this investigation. The coating material was supplied and applied by Matrix Composite Engineering. The metallic substrates were carbon steel (A106 Grade B) and UNS S31603 (316L SS) stainless-steel pipes. Table 1 lists the nominal chemical compositions of the substrate materials. The pipe dimension was 350 mm in length, 101.6 mm in diameter, and 6 mm in thickness. Both substrates were subject to surface cleaning to a Sa 2.5 standard, followed by a spray coating application to achieve a relatively uniform dry film thickness (DFT). The DFT was measured using a DeFelsko DFT digital gauge. The DFT values averaged from 10 measurements were 512 ± 24 μm on carbon steel, and 722 ± 68 μm on 316L-SS, which was within the products' specification, as shown in Table 2.

2.2. Experimental setup

The test apparatus was modified based on a test setup developed by Halliday et al. [16]. The modified test setup is schematically shown in Fig. 1. The coated pipe was insulated with a 50 mm thick mineral wool insulation and further jacketed using aluminium foil as an external cladding. Mineral wool insulation was selected in this study as it is the most common insulation [17]. The pipe was placed vertically on top of a hot plate, which was set to 200 °C. Thermocouples were installed to monitor coating surface temperature in-situ at 0 mm, 75 mm, 150 mm, 225 mm, and 350 mm away from the bottom of the pipe.

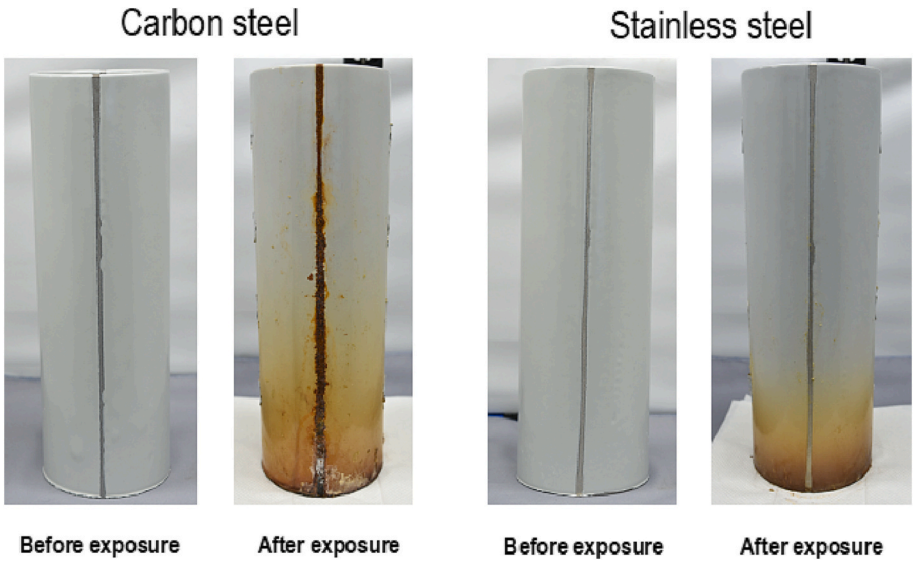

Fig. 5. Surface morphology of coated vertical pipes (coated carbon steel and stainless steel) before and after 30 cycles of CUI cyclic exposure at elevated temperatures.

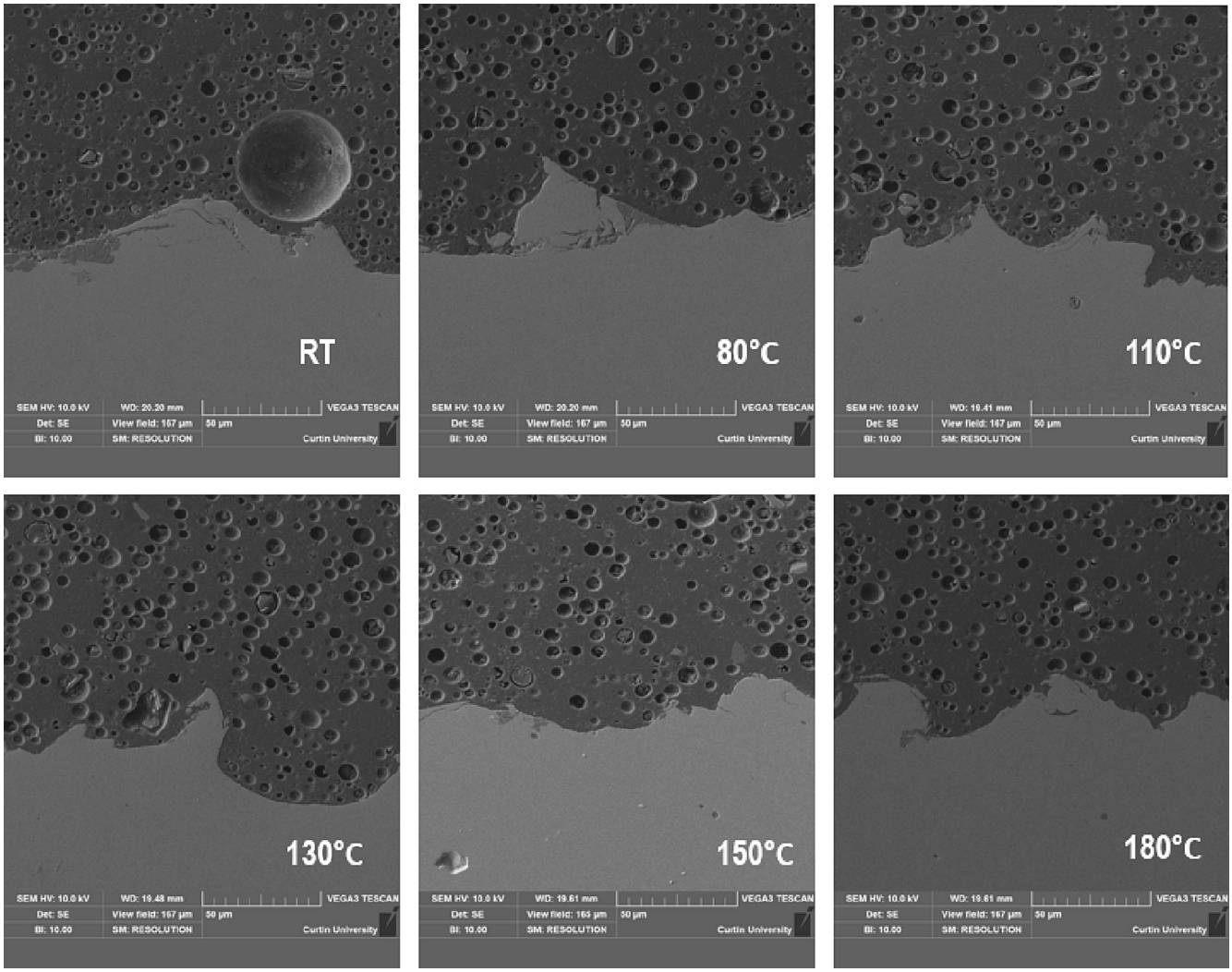

Fig. 6. SEM images of cross-sectional area of coating on carbon steel exposed at room temperature to 180 °C.

In total, 30 thermal cycles were completed for coating performance evaluation in an accelerated CUI test, with each thermal cycle consisting of 6 h of heating and 18 h of cooling. One liter of 1 % (m/V) NaCl solution was constantly introduced into the insulation from the top, at a rate of 80 mL per hour, following the end of the daily 6 h heating period. A tray and container were used to collect the solution that was leached from the insulation. Thus, the amount of solution that had been absorbed and retained within the insulation (water evaporation was considered negligible) was obtained. Two 6-mm artificial lines were scribed along the overall length of the pipe, in the opposite position, to facilitate the determination of susceptibility of coating delamination before and after thermal exposure.

2.3. Pull off adhesion and peel-off test

The adhesion property of a coating refers to the bonding strength between the coating and its substrate [18]. Apparent adhesion strength, which is commonly used to evaluate and compare coating performance among industry, was measured using pull-off adhesion test as per ASTM D4541 [19]. 14 mm Aluminium dollies were polished to #240 grit SiC paper, degreased using ethanol to remove superficial dust and contaminants, and then immersed in the adhesion promoter solution ((3-glycidyloxypropyl)trimethoxysilane) for 5 min. The adhesion promoter helped reduce the possibility of glue failure (i.e., a disbondment between dolly/glue or glue/coating interfaces), which is considered an invalid result. The coating surface was slightly abraded using #1200 SiC grit SiC paper to increase the surface profile and wiped clean using ethanol to remove debris. Afterwards, the dollies were adhered to the coating surface using a two-component epoxy adhesive (Araldite high-strength). After the glue was cured for 24 h, a self-aligning adhesion tester (PosiTector, PosiTest AT-A) was used to conduct testing on the dollies at a pull-off rate of 4 MPa/s. Adhesion tests were repeated in triplicate before and after exposure, to determine the failure mode and pull-off adhesion strength of coatings in each exposure scenario.

The peel-off test was performed to determine the extent of coating delamination according to ASTM D6677 using a utility knife, with a modified approach. A sharp utility knife was employed to lift the coating from its substrate, from four directions at each side of the scribe, with a scribing length limited at 10 mm. The lift-up process was stopped when “obvious resistance” was found. The comparative lift-up area due to loss of adhesion was recorded and calculated in % in a specified 40 × 30 mm rectangular area.

2.4. Chemical analysis using Fourier transform infrared spectroscopy (FTIR)

FTIR spectra of the exposed coating were obtained using Nicolet iS50 FTIR instrument under a single-bounce diamond attenuated total reflectance (ATR) mode. Test specimens were prepared by scraping approximate 2 mg powder samples from the coated pipes. 64 scans were

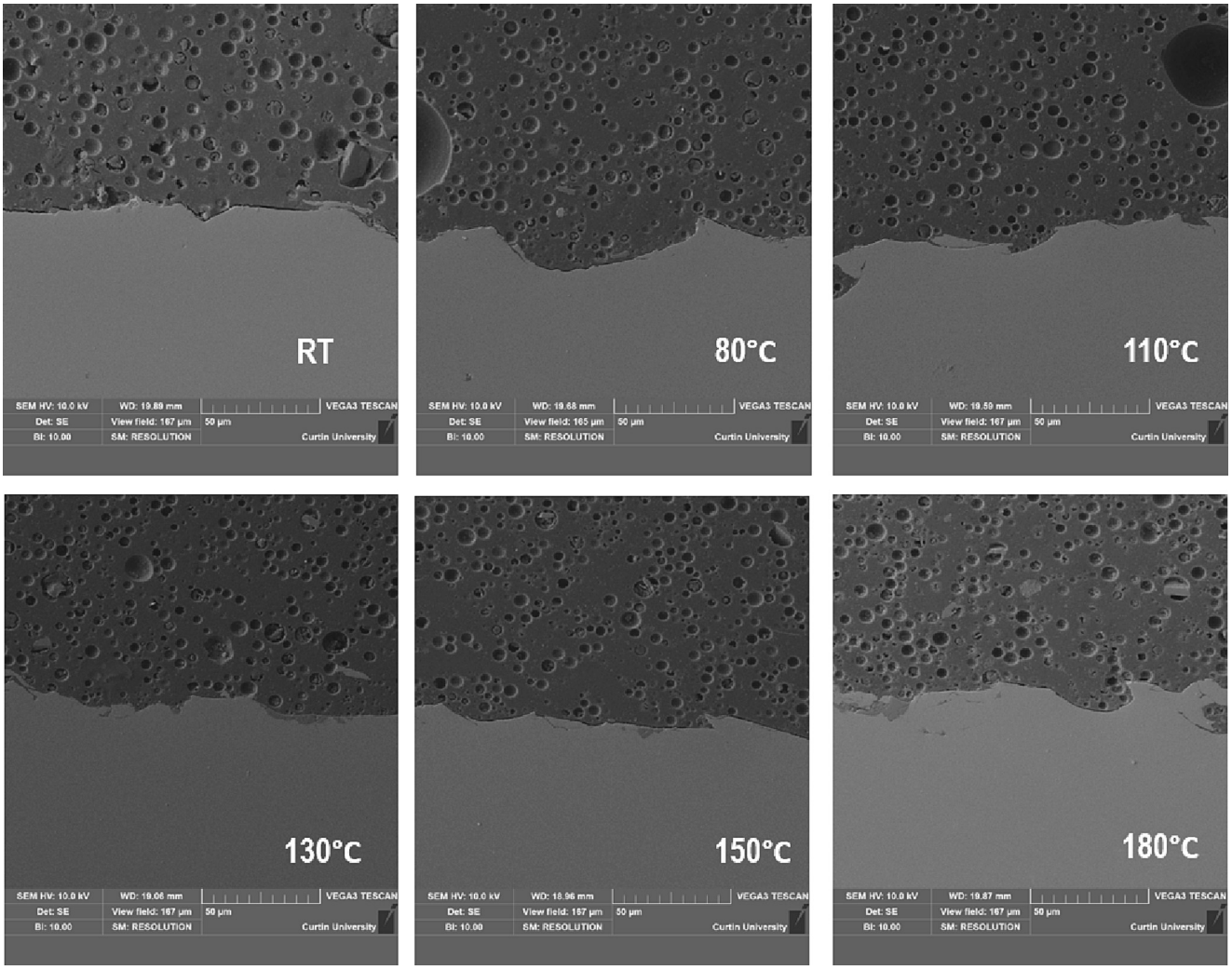

Fig. 7. SEM images of cross-sectional area of coating on stainless steel exposed at room temperature to 180 °C.

averaged for each spectrum collected over a range of wavenumbers from 400 to 4000 cm^{-1} at a resolution of 4 cm^{-1}. Data were analysed using OPUS software.

2.5. Differential scanning calorimetry (DSC)

DSC was performed on a TA Instruments DSC 25 differential scanning calorimeter to determine the glass transition temperature of coatings exposed at different temperatures. An approximate 3 mg powder sample was weighed into a standard aluminium sample pan, and a standard aluminium lid was crimped in the inverted position. A matched empty pan was used as a reference. The sample was heated from 25 to 200 °C at 10 °C/min in a nitrogen atmosphere flowing at 50 mL/min. The sample was cooled at 20 °C/min back to 25 °C. The temperature scale of the instrument was calibrated using the phase transition of 99+ % adamantane (−65.54 °C), 18.2 MΩ·cm water (0.010 °C), 99.999 % indium (156.60 °C), and 99.99+ % tin (231.93 °C). The cell constant was determined using the heat of fusion of 99.999 % indium (28.47 J/g).

2.6. Electrochemical impedance spectroscopy (EIS) characterisation

Square specimens (50 mm by 50 mm) were cut from the vertical pipe after the thermal exposure tests (30 cycles) were completed. EIS measurements of the polyamine-cured epoxy coated metal were performed using a customised three-electrode cell made from a polyvinyl chloride (PVC) cup, shown in Fig. 2. Herein, the coated metal was the working electrode with a surface area of 11.34 cm^2, a saturated silver/silver chloride (Ag/AgCl) served as the reference electrode with a Luggin capillary (in close proximity to the working electrode) filled with 3 M KCl, and a graphite rod used as the counter electrode. The test solution was 3.5 wt% NaCl, unadjusted pH = 6.5 ± 0.2. All the experiments were carried out using a Gamry Ref 600+ potentiostat. A sinusoidal AC perturbation with a 20 mV amplitude vs open circuit potential (OCP) used. The scanning frequency ranged from 100 kHz to 0.01 Hz. Data was collected at 6 points per decade.

2.7. Scanning electron microscopy (SEM)

The cross-sectional area of coated steel specimens was characterised using Tescan Vega3 VP scanning electron microscope. SEM was used to examine potential coating delamination, i.e., micro-cracks at the coating-metal interface, which cannot be observed at lower magnifications but may have developed due to thermal exposure. The cross-sectional surfaces were prepared by polishing sample surfaces down to 1 μm using diamond paste, cleaned using ethanol in an ultrasonic vibration bath and wiped dry. All the images were captured under SEM at a constant working distance of 20 mm with an acceleration voltage of 10 kV and a beam current of 10 A.

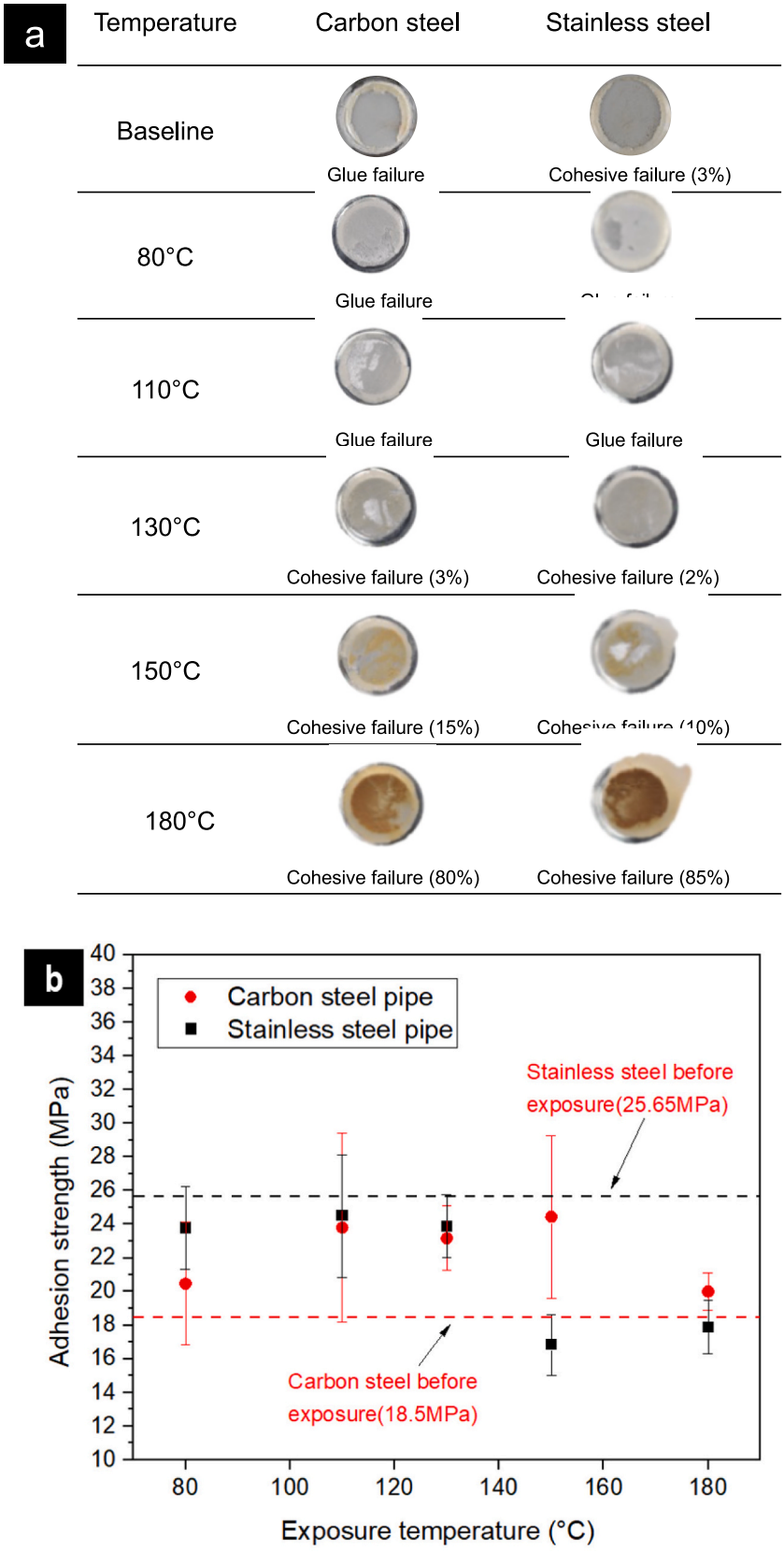

Fig. 8. Pull-off adhesion test to evaluate coating adhesion behaviour: (a) adhesion strength and (b) failure mode, before and post heat treatment at different temperatures.

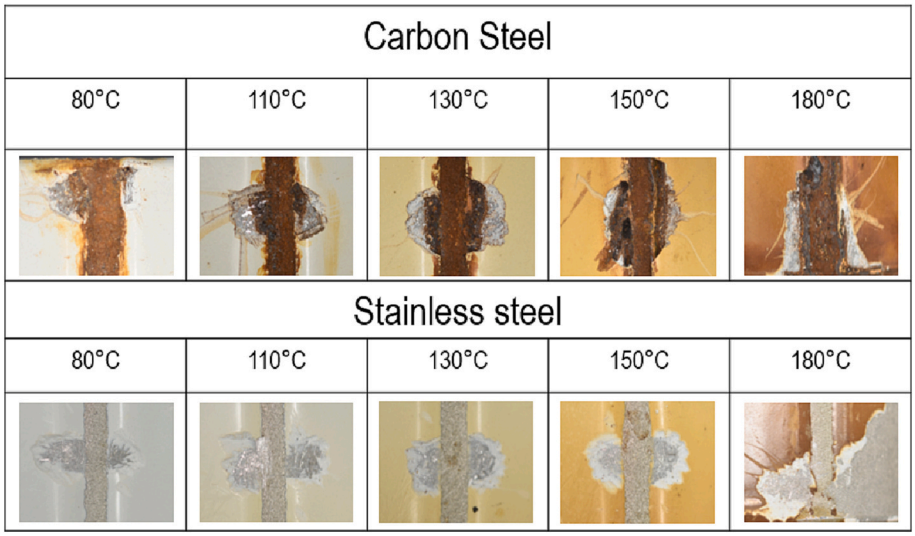

Fig. 9. Evaluation of coating adhesion by knife, according to ASTM D6677 with a modified approach, on carbon and stainless steel pipes after thermal exposure at different temperatures 80–180 °C to study the bonding properties.

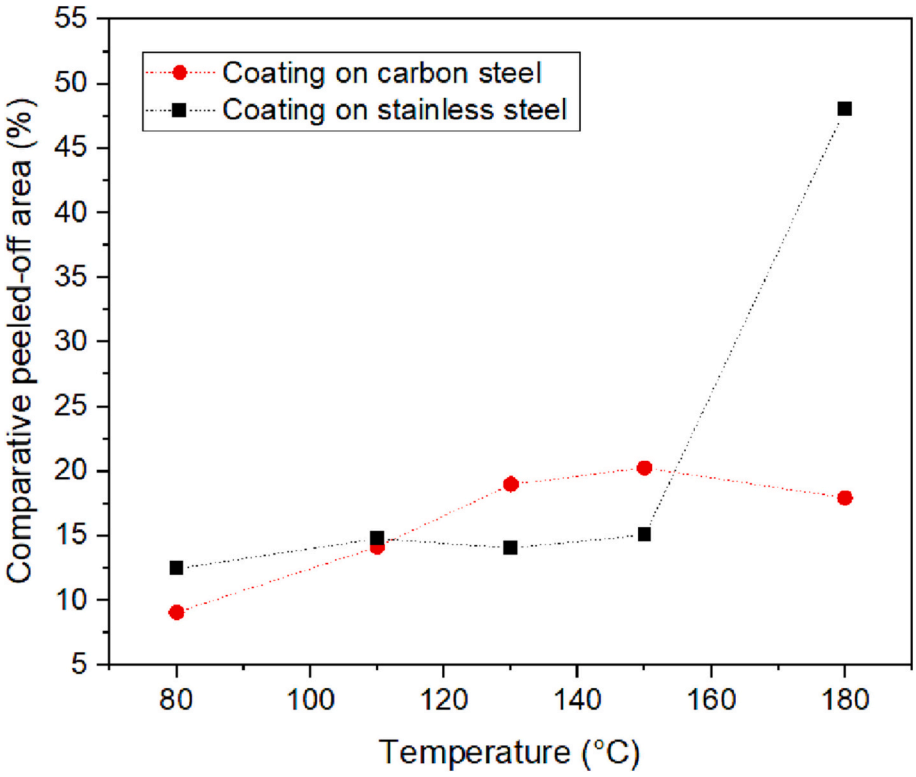

Fig. 10. Comparative peeled-off coating area, in %, from carbon steel and stainless steel substrates after exposed at different temperatures.

3. Results and discussion

3.1. Insulation water retention

Prolonged exposure to moisture was shown to be one of the critical factors leading to epoxy coating degradation [20–22]. Thus, it was crucial to ensure that the quantity of water absorbed by the insulation was comparable between the carbon steel and stainless steel pipes. In this study, the amount of retained solution within thermal insulation was recorded on days 5, 10, 15, 20, 25, and 30, as plotted in Fig. 3. It was indicated that the amount of water uptake within the insulation on carbon and stainless steel was comparable and increased, from 30 % to 60 %, when exposure time increased from 5 to 30 days. The phenomenon was in line with findings from another study, which showed an increased moisture diffusion capability (moisture diffusivity) when the insulation was subjected to prolonged water/moisture exposure [21].

3.2. Temperature profile, visual appearance, and cross-sectional morphology

The surface temperature of the coatings was recorded daily at 0, 75, 150, 225, 300, and 350 mm away from the bottom of the pipes, i.e., the

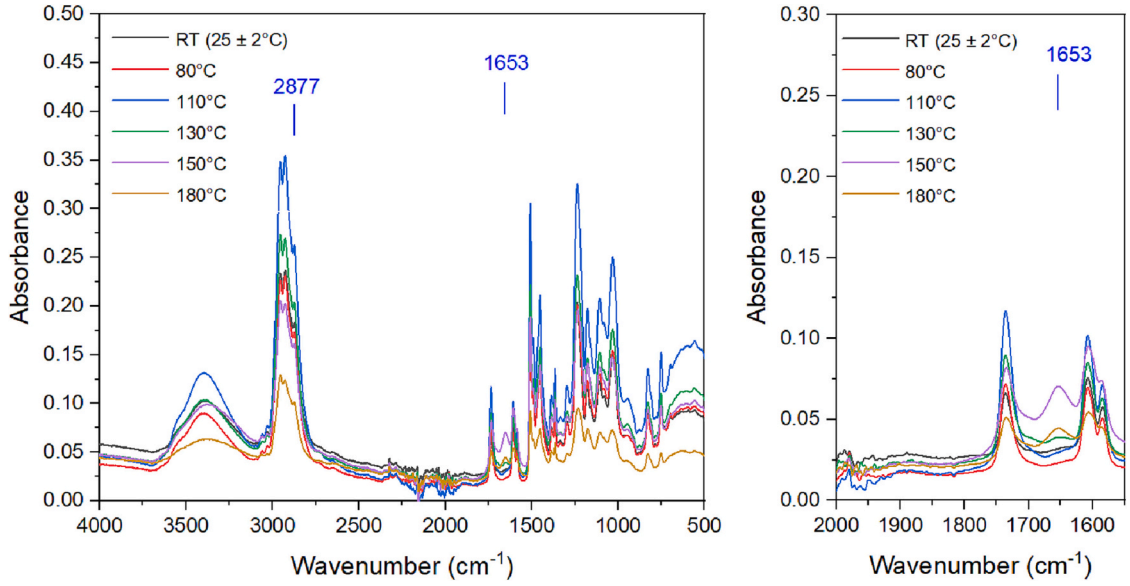

Fig. 11. FTIR spectra of coating specimens retrieved from coated carbon steel pipe, before and after thermal exposure, at temperatures from 25 ± 2 °C to 180 °C. (a) Spectra plotted over a range of wavenumbers from 400 to 4000 cm^{-1}, and (b) spectra plotted over a range of wavenumbers from 1550 to 2000 cm^{-1}.

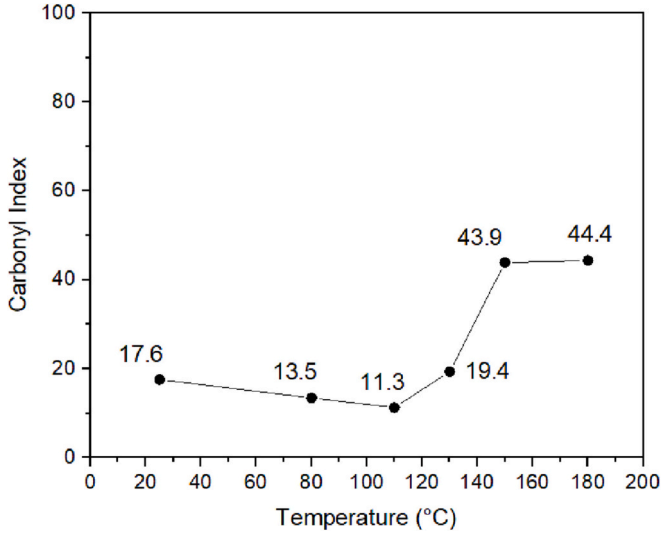

Fig. 12. Carbonyl index of an epoxy coating applied on a carbon steel substrate as a function of exposure temperatures.

hot plate heat source. Fig. 4 compares the average temperature profiles of the coatings along the longitudinal section of the two pipes. A relatively rapid temperature decrease was noticed in the coated stainless steel compared to the coated carbon steel due to the difference in the thermal conductivity of carbon steel (45 $W{\cdot}m^{-1}{\cdot}K^{-1}$) and stainless steel (15 $W{\cdot}m^{-1}{\cdot}K^{-1}$). Overall, the temperature profile of the coatings ranged from 200 to 50 °C. The temperature gradient was wide enough to study the thermal degradation of polyamine-cured epoxy coatings.

Fig. 5 shows the appearance of the coatings before and after thermal cycling exposure. The visual examination revealed no visible cracks or blistering. However, discolouration was observed, starting from the bottom sections of both coated pipes. Rusting was apparent from the scribed region on coated carbon steel pipe; however, no evidence of coating delamination or cracks was observed on coated stainless-steel pipe based on visual inspection.

Cross-sectional SEM was used to characterise the morphology of potential delamination and cracks that could occur at the microscale. Thermal exposure is known to introduce thermal stresses due to the mismatch of the coefficients of thermal expansion of different materials (i.e., coating and metallic substrate) [22,23]. Therefore, microcracks may develop at the metal/coating interface under thermal cycling conditions [24,25]. As shown in Figs. 6 and 7, no clear signs of cracks were observed on the coated carbon and stainless steel specimens, indicating that, under the current experimental conditions, thermal cycling-induced thermal stress had no impact on the micro-cracks formation.

3.3. *Pull-off adhesion and peel-off testing*

Adhesion tests were performed at various locations along the pipes corresponding to exposure temperatures of 80, 110, 130, 150, and 180 °C. On the coated carbon steel pipe, adhesion tests were performed at 28, 75, 150, 225, and 350 mm from the bottom of the pipe. On the stainless steel pipe, tests were conducted at 28, 56, 94, 130, and 225 mm from the bottom of the pipe. At each location, pull-off adhesion tests were conducted in triplicate. The failure modes and adhesion strength values are shown Fig. 8 (a–b).

The baseline pull off adhesion values were 18.5 MPa and 25.7 MPa for carbon and stainless steel, respectively. Glue failure was predominantly observed, suggesting that the cohesive strength of the coating or the adhesion strength of the coating and the substrate were greater than the reported values.

After the exposure up to 130 °C, no measurable change was observed on both carbon and stainless steel, as demonstrated by the absence of substantive increase in cohesive or adhesive failure or the reduction in adhesion values. The percentage of cohesive failure mode slightly increased to 15 and 10 % when exposed to 150 °C and markedly rose to 80 and 85 % at 180 °C, for carbon and stainless steel, respectively. The transition from glue to cohesive failure indicated that the cohesive strength of the coating reduced to below that of the glue.

The adhesion values of the coating on carbon steel were not affected by the thermal exposure, as shown in Fig. 8b. High adhesion values were obtained on carbon steel surfaces at all exposure temperatures, including at 180 °C. A similar behaviour was observed on the stainless steel up to 130 °C. However, at 150 and 180 °C, a sharp drop in adhesion values was observed (i.e., from 24 to 16 MPa), along with a progressive increase in cohesive failure. It appears that the stainless steel substrate facilitated the loss of coating adhesion.

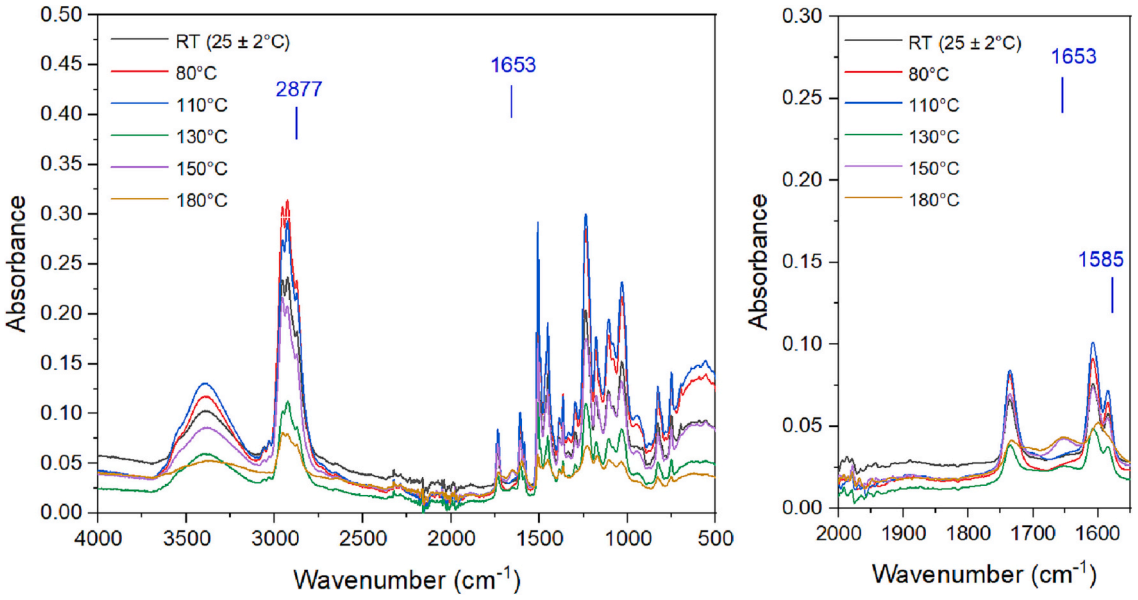

Fig. 13. FTIR analysis of polyamine-cured epoxy coatings, retrieved from coated stainless steel samples, exposed at from room temperature to 180 °C, with new absorption band identified at ~1653 cm^{-1} wavenumber, when coating was exposed at above 130 °C. Spectrum of pre-exposure sample at room temperature (25 ± 2 °C) was presented as a control baseline composition.

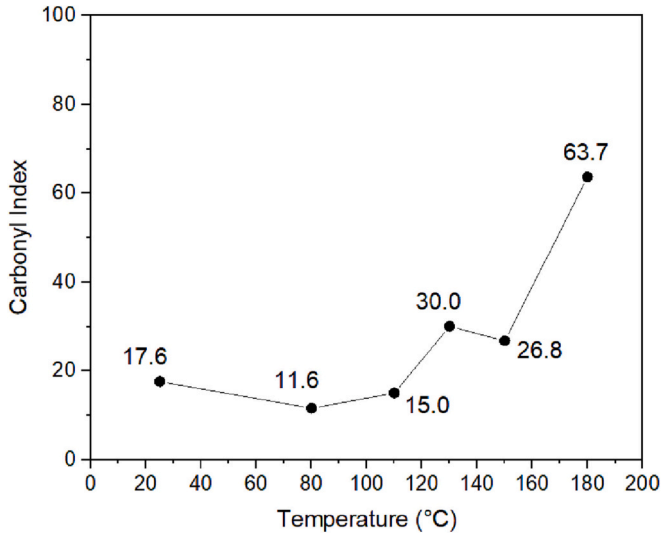

Fig. 14. Carbonyl index of an epoxy coating applied on a stainless steel substrate as a function of exposure temperatures.

A relatively similar peeled-off coating area, in %, was lifted by knife on coated steel samples exposed from 80 to 150 °C. When the exposure temperature reached 180 °C, the bonding strength between the coating layer and stainless steel substrate appeared to be significantly reduced with up to 50 % of the coating area lifted up and removed, as shown in Fig. 9. The peel-off adhesion strength between the coating and metallic substrate decreased drastically at high temperatures, especially on the stainless steel substrate, as shown in Fig. 10.

3.4. FTIR results

Fig. 11 shows the FTIR spectra of coating samples retrieved from the carbon steel pipe before and after thermal exposure at room temperature (25 ± 2 °C), 80, 110, 130, 150, and 180 °C. All the significant bands located above 1000 cm^{-1} wavenumbers were identified. Bands located at 3380 cm^{-1} were identified from specimens exposed at all temperatures and they were attributed to O—H stretching of the hydroxyl group, potentially from water molecules or from oligomer with low degree of polymerisation [26,27]. Absorption bands located at approximately 2960 cm^{-1} and 2930 cm^{-1} corresponded to —CH_2 and —CH_3 stretching vibration modes of aromatic and aliphatic chains, respectively [28]. Bands with wavenumber at 1736 cm^{-1} were related to C═O stretching. Absorption bands located at 1508 cm^{-1} with medium to strong intensity were identified to be the C—C stretching vibrations due to the presence of aromatic rings in the monomer backbone chain, and bands located at 1452 cm^{-1} was assigned to the C—H bending of alkane. In addition, bands located at 1296 cm^{-1} and 1178 cm^{-1} were related to the C—O bonding stretching vibrations in the ether linkage of an aromatic ring. Bands at 1108 cm^{-1} and 1033 cm^{-1} corresponded to aromatic stretching and C—O—C stretching of the ether linkage, respectively.

A new absorption band was identified at the wavelength of ~1653 cm^{-1} when the exposure temperature was above 150 °C. This new band was assigned to the C═O stretching of carbonyl group in amide species and was associated with the amine-related aging mechanism [13,14]. Carbonyl formation was previously identified as the root cause of the discolouration/yellowing of polyamine-cured epoxy [15]. While the yellowing of epoxy induced by UV exposure is reversible, discoloration caused by the formation of carbonyl due to thermo-oxidation is permanent. Examples of such groups are quinone-like structures formed during the oxidation of the aromatic moiety in the polymeric backbone [29]. In this experiment, the discolouration of epoxy did not reverse after heat exposure, indicating the process was an irreversible property alteration. However, the correlation between the extent of thermal oxidation and the overall integrity of the epoxy coated system is not clear.

Carbonyl index was used to indicate the severity of oxidation for polymers in an accelerated weathering condition [30] and to evaluate the level of degradation in polymeric systems [30,31]. The carbonyl index was determined using Eq. (1), by dividing the band's intensity at 1653 cm^{-1} by that at 2877 cm^{-1} (reference peak, methylene —CH_2 group). The carbonyl index of the specimens exposed at different temperatures was calculated and plotted in Fig. 12. An increasing carbonyl index number was observed at higher temperatures (>130 °C). The carbonyl index reached 44.2 for coated carbon steel samples exposed above 150 °C, compared with 17.6 for coatings without thermal

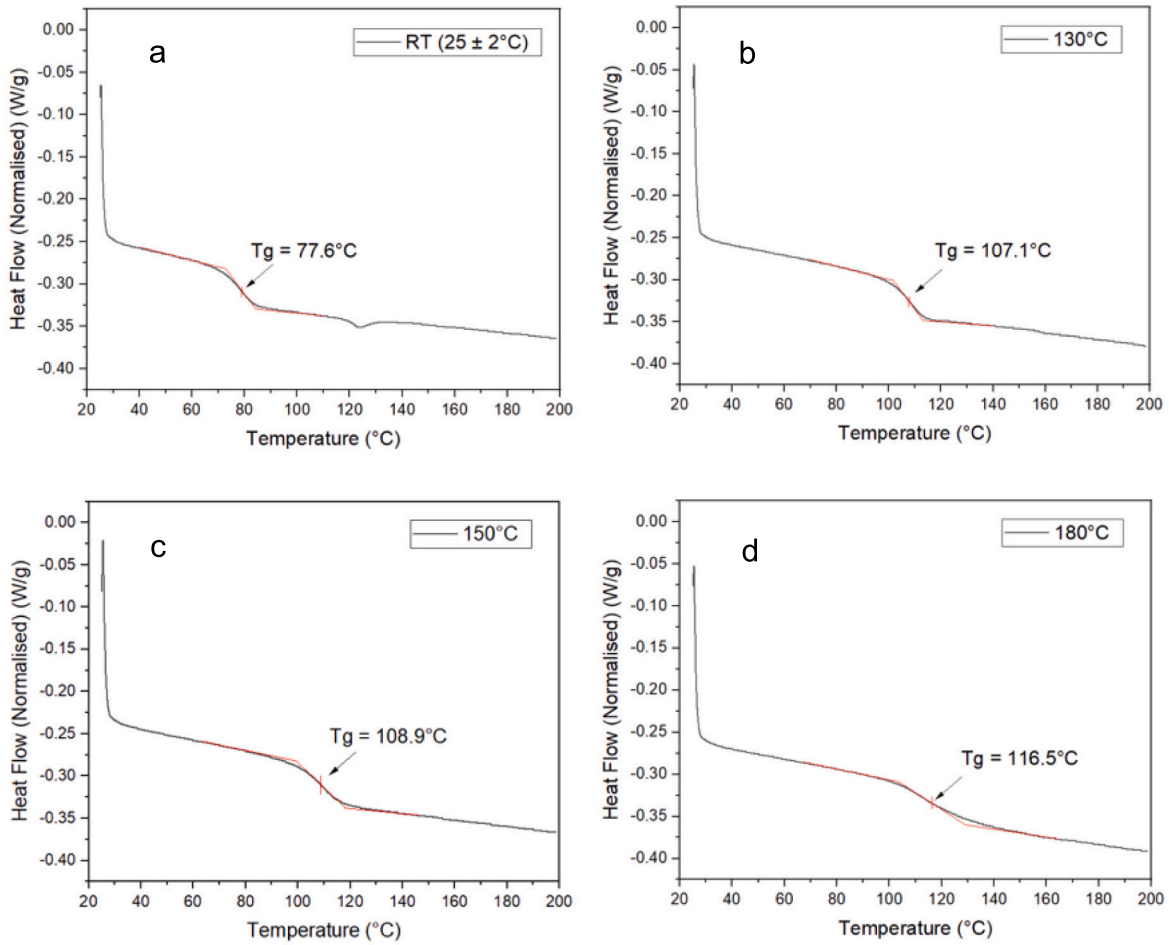

Fig. 15. Glass transition temperature measurements using DSC for coating specimens exposed at different temperatures (a) 25 ± 2 °C, (b)130 °C, (c)150 °C, and (d) 180 °C. An increase of Tg value was observed when coating exposure temperature increases.

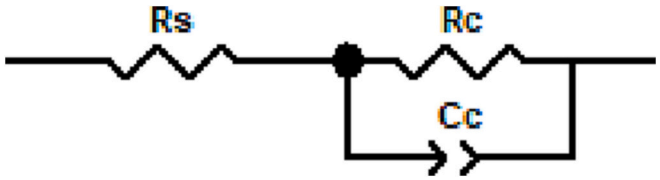

Fig. 16. Electrical equivalent circuit used to fit EIS data in this study.

exposure. A higher carbonyl index value indicated a higher level of chain scission and, consequently, more yellowing [27]. Thus, under prolonged thermal cyclic, CUI exposure above 150 °C led to coating thermal degradation.

$$\text{Carbonyl Index}\left(1653\ \text{cm}^{-1}\right) = \frac{I_{\text{adsorbance at 1653 cm}^{-1}}}{I_{\text{adsorbance at 2877 cm}^{-1}}} \times 100\% \quad (1)$$

Fig. 13 shows the FTIR spectra of coating samples retrieved from a stainless steel pipe before and after thermal exposure, at room temperature (25 ± 2 °C), 80, 110, 130, 150, and 180 °C. The allocation of absorption bands was similar as the bands identified from coated carbon steel. A new band located at wavelength of ~1653 cm^{-1} was additionally identified above 130 °C. A reduction of band intensity of ~1585 cm^{-1}, especially at an exposure temperature 180 °C, suggested the oxidation reaction from hydroxyl to carbonyl. As with the coated carbon steel case, the carbonyl index increased with exposure temperatures, as shown in Fig. 14. The highest value of carbonyl index, i.e., 63.7, was measured at 180 °C, indicating that a certain level of chain scission and degradation had occurred. The carbonyl index measured from coated carbon steel and stainless steel at the same exposure temperatures was differed. The difference can be attributed to the minor temperature variation in the test locations. As such, the level of chemical degradation within a specific test point can vary slightly, leading to a numerical difference. Nevertheless, in both cases, the carbonyl index followed the same trend, increasing with increasing exposure temperature. The carbonyl index calculated from the coating's FTIR spectra reached a maximum at 180 °C on both substrates.

3.5. Glass transition temperature

DSC was used to determine the glass transition temperature (T_g) of coating samples exposed to room temperature, 130, 150, and 180, as shown in Fig. 15 (a–d). In this study, chemical changes occurring to the coating are driven predominantly by temperature and moisture, the samples were thus taken from the coated carbon steel substrates only. T_g was determined from the second heating cycle thermograph, at the half height midpoint of the intersection of tangent lines determined from the first and second temperature transitions. A significant increase in T_g values, from 77.6 °C to 116.5 °C, was found when the coating was exposed from 25 °C to 180 °C.

An increase in T_g indicates a restrictive segmental motion of polymeric chains and a simultaneous decrease of free volume in the polymeric system [32]. The decrease in polymeric free volume may be related to the additional formation of bulky and inflexible side groups or

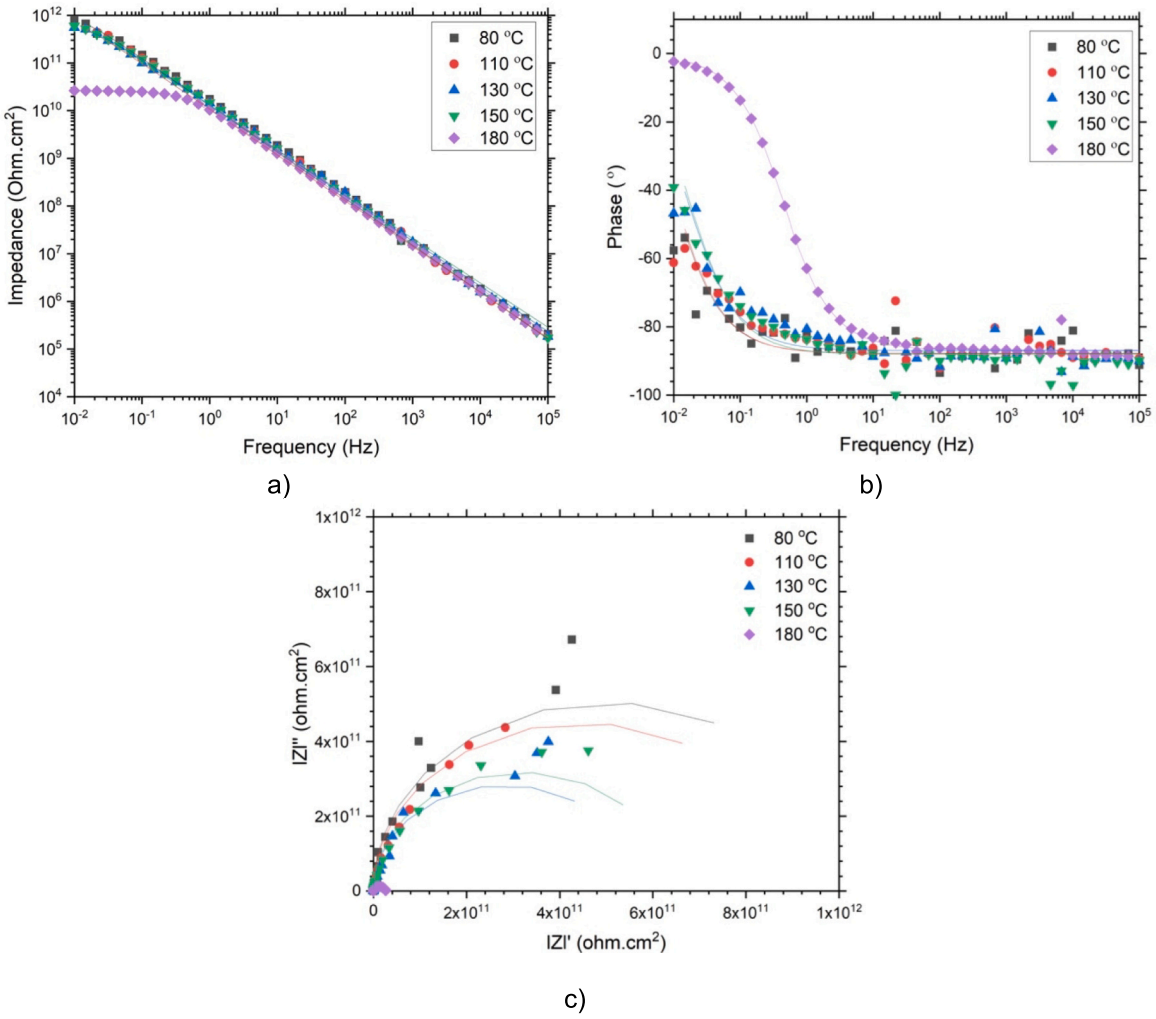

Fig. 17. Bode plots of polyamine-cured epoxy coating on carbon steel, after exposure in 3.5 wt% NaCl solution for 4 days. a) lZl and b) phase angle vs log(frequency) and c) Nyquist plot. Markers are experimental data and lines are fitting.

Table 3
Resistance and coating CPE parameter values derived from EIS fitting analysis on the coated carbon steel systems used to calculated %water uptake within coatings that exposed at 80 °C–180 °C.

Temperature	CPE-Q (F cm^{-2})	CPE-n	R_c (Ω cm^2)
80 °C	1.25×10^{-10}	0.97	1.11×10^{11}
110 °C	1.35×10^{-10}	0.98	9.93×10^{10}
130 °C	1.43×10^{-10}	0.97	6.24×10^{10}
150 °C	1.37×10^{-10}	0.98	6.24×10^{10}
180 °C	1.93×10^{-10}	0.95	2.33×10^{9}

an increase in the molecular weight [33]. However, no exothermic event was present in the DSC spectra, indicating no additional cross-linking activity and no major increase in molecular weight. The formation of carbonyl group, as a bulky additional polar group, in this case, can be responsible for the increased T_g value. However, the interrelationship between the formation of new compounds at high temperature and the subsequent change of T_g requires further investigation.

3.6. Electrochemical impedance spectroscopy

An open-lead measurement was firstly performed to determine the highest impedance that the current experimental setup can attain, which also provides information on the system's capability to measure an intact coating. Under the current experimental setting and instrument, the open lead spectrum of the system's impedance value at low frequency (0.01 Hz) approximately equals to 10^{13} Ω.

After the exposure, EIS tests were performed on coated specimens in 3.5 wt% NaCl. The samples were immersed in the test electrolyte for 4 days at room temperature (22 ± 2 °C). The EIS spectra were fitted with an electrical equivalent circuit presented in Fig. 16. The spectra obtained from the coated carbon steel and stainless steel are shown in Figs. 17 and 18, respectively. Samples exposed to temperatures up to 150 °C had a capacitive behaviour. The total low frequency impedance, $Z_{0.1Hz}$, was close to 10^{12} Ω·cm^2. When the coating was exposed to 180 °C, phase shift occurred at higher frequency and the total impedance at low frequency decreased by an order of magnitude to 10^{11} Ω·cm^2. This behaviour has been associated with an electrolyte diffusion into the coating matrix [34,35].

In Fig. 17 markers represent experimental results, while solid lines indicate the model fitting. A constant phase element (CPE) was used instead of a capacitor to represent the dielectric properties of the coating. The CPE component has been associated with inhomogeneous electrolyte uptake [36] and was found to be suitable where a large coating resistance is anticipated. Table 3 shows the results of the equivalent circuit fitting. As seen in Table 3, R_c decreased with temperature, suggesting an onset of barrier protection deterioration at high temperature. The CPE marginally increased with increasing exposure temperature but remained within the same order of magnitude.

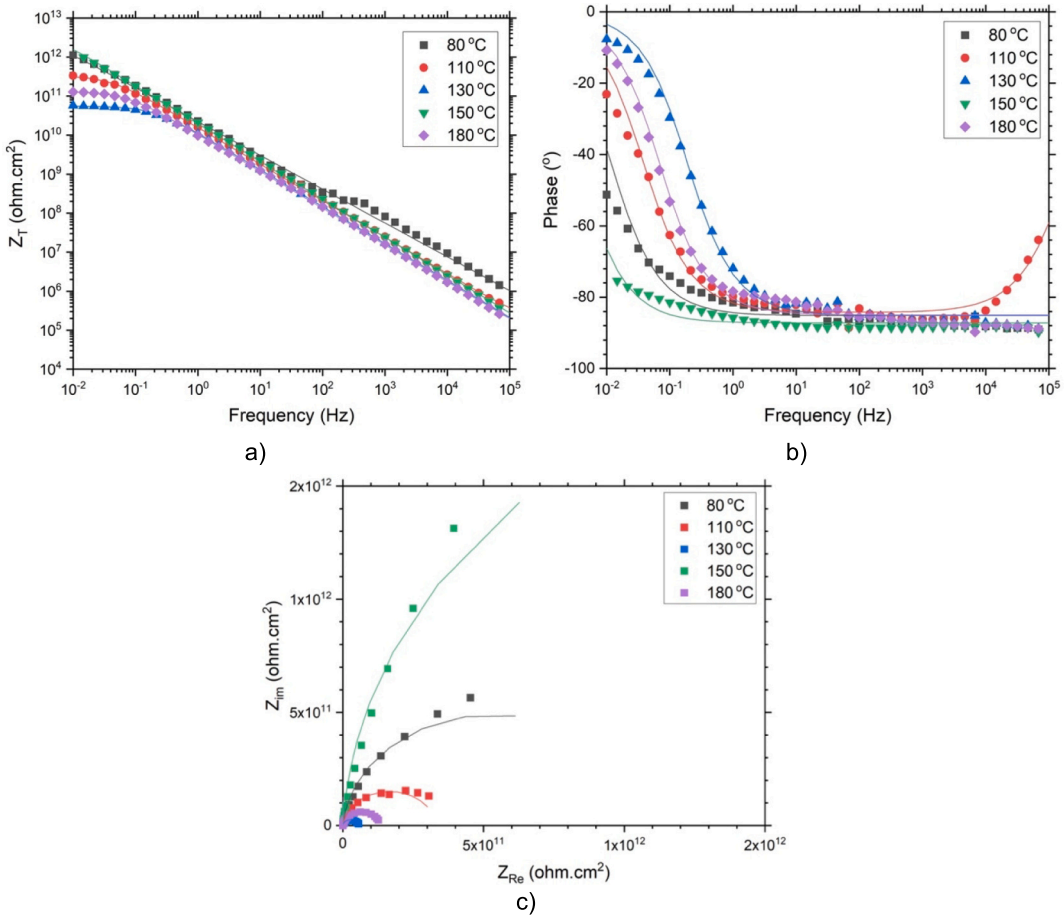

Fig. 18. Bode plots of polyamine-cured epoxy coating on stainless, after exposure in 3.5 wt% NaCl solution for 7 days. a) lZl and b) phase angle vs log(frequency) and c) Nyquist plot. Markers are experimental data and lines are fitting.

Table 4
Resistance and coating CPE parameter values derived from EIS fitting analysis on the coated stainless steel systems.

Temperature	R_s (Ω cm^2)	CPE-Q (F cm^{-2})	CPE-n	R_c (Ω cm^2)
80 °C	20	1.24×10^{-10}	0.95	9.43×10^{10}
110 °C	50	1.29×10^{-10}	0.94	2.94×10^{10}
130 °C	30	1.73×10^{-10}	0.95	4.83×10^{9}
150 °C	60	9.74×10^{-10}	0.97	3.85×10^{11}
180 °C	30	1.92×10^{-10}	0.94	1.15×10^{10}

For coated stainless steel, the electrochemical impedance spectra are shown in Fig. 18 (a–c) and the equivalent circuit fitting results are shown in Table 4. Overall, the coating exhibited similar behaviour as shown in carbon steel, i.e., high barrier protection was observed as evident by the high coating impedance. The coating impedance fluctuated from 10^9 to 10^{11} Ω·cm^2.

4. Conclusions

The behaviour and degradation of a polyamine-cured epoxy coating was studied at elevated temperatures on carbon and stainless steel substrates insulated with mineral wool. The following conclusions were drawn from the results presented herein:

I. The pull off adhesion strength was not affected by the CUI thermal exposure. However, there was an increase in cohesive coating failure when the exposure temperature was >130 °C, suggesting the deterioration of the coating integrity.
II. Chemical degradation of the amine-cured epoxy coating exposed at temperatures above 130 °C was identified by the irreversible formation of the carbonyl functional group and an increase in T_g from 77.6 °C to 116.5 °C.
III. Prolonged thermal exposure at high temperature up to 150 °C led to a decline in the low-frequency total impedance; however, no changes in coating capacitance were observed as a function of temperature.
IV. The metal substrates played no measurable role in barrier coating performance under the conditions tested.

CRediT authorship contribution statement

Qing Cao: Investigation, Methodology, Writing – original draft. **Ibukun Oluwoye:** Writing – review & editing. **Thunyaluk Pojtanabuntoeng:** Conceptualization, Supervision, Writing – review & editing. **Hanan Farhat:** Supervision, Funding acquisition. **Mariano Iannuzzi:** Supervision, Writing – review & editing.

Declaration of competing interest

Qing Cao reports financial support was provided by Qatar Environment and Energy Research Institute.

Data availability

Data will be made available on request.

Acknowledgments

The authors would like to thank Qatar Environment and Energy Research Institute QEERI Corrosion Centre for their financial support and permission in publishing this paper.

References

[1] V.M. Liss, in: Preventing Corrosion Under Insulation 94, Natl. Board Boil. Press. Vessel Insp, 1998, pp. 97–98.
[2] S. Winnik, Corrosion Under Insulation (CUI) Guidelines, 2nd ed., Elsevier, Cambridge, UK, 2015.
[3] J.F. Delahunt, Corrosion under thermal insulation and fireproofing - an overview, Corrosion (2003) 1–10.
[4] D. Kotnarowska, Influence of ultraviolet radiation and aggressive media on epoxy coating degradation, Prog. Org. Coat. 37 (1999) 149–159.
[5] C. Zhang, W. Li, C. Liu, C. Zhang, L. Cao, D. Kong, W. Wang, S. Chen, Effect of covalent organic framework modified graphene oxide on anticorrosion and self-healing properties of epoxy resin coatings, J. Colloid Interface Sci. 608 (2022) 1025–1039.
[6] M. Mirzaee, M. Rezaei Abadchi, A. Fateh, A. Zolriasatein, Investigation of corrosion properties of modified epoxy and polyurethane organic coating on steel substrate, Prog. Color. Color. Coat. 15 (2022) 25–36.
[7] J.P. Ault, The use of coatings for corrosion control on offshore oil structures, J. Prot. Coat.Linings 23 (2006).
[8] ISO 19277:2018, Petroleum, Petrochemical and Natural Gas Industries — Qualification Testing and Acceptance Criteria for Protective Coating Systems Under Insulation, 2018.
[9] API 583:2014, Corrosion Under Insulation and Fireproofing, 2014.
[10] Corrosion Under Insulation (CUI) Guidelines: (EFC 55), G. Landtsheer, 2020.
[11] H. Zargarnezhad, E. Asselin, D. Wong, C.N. Lam, A critical review of the time-dependent performance of polymeric pipeline coatings: focus on hydration of epoxy-based coatings, Polymers 13 (2021) 1517.
[12] B. Mailhot, S. Morlat-Therias, M. Ouahioune, J. Gardette, Study of the degradation of an epoxy/amine resin - 2, Macromol. Chem. Phys. 206 (2005) 575–584.
[13] S. Morsch, Y. Liu, S.B. Lyon, S.R. Gibbon, B. Gabriele, M. Malanin, K.J. Eichhorn, Examining the early stages of thermal oxidative degradation in epoxy-amine resins, Polym. Degrad. Stab. 176 (2020), 109147.
[14] Y.C. Lin, X. Chen, H.J. Zhang, Z.P. Wang, Effects of hygrothermal aging on epoxy-based anisotropic conductive film, Mater. Lett. 60 (2006) 2958–2963.
[15] A.E. Krauklis, A.T. Echtermeyer, Mechanism of yellowing: carbonyl formation during hygrothermal aging in a common amine epoxy, Polymers 10 (2018) 1–15.
[16] M. Halliday, Development & testing of new generation high temperature corrosion resistant coatings, Corrosion (2005) 1–8.
[17] Q. Cao, T. Pojtanabuntoeng, M. Esmaily, S. Thomas, M. Brameld, A. Amer, N. Birbilis, A review of corrosion under insulation: a critical issue in the oil and gas industry, Metals 12 (2022) 561.
[18] H. Wei, J. Xia, W. Zhou, L. Zhou, G. Hussain, Q. Li, K.K. Ostrikov, Adhesion and cohesion of epoxy-based industrial composite coatings, Compos. Part B Eng. 193 (2020) 1–20.
[19] ASTM D4541, Standard Test Method for Pull-off Strength of Coatings Using Portable Adhesion Testers, ASTM International, West Conshohocken, Pennsylvania, 2017.
[20] D.R. Lefebvre, K.M. Takahashi, A.J. Muller, V.R. Raju, Degradation of epoxy coatings in humid environments: the critical relative humidity for adhesion loss, J. Adhes. Sci. Technol. 5 (1991) 201–227.
[21] J. Abenojar, M.A. Martinez, F. Velasco, J.C. Del Real, Effect of moisture and temperature on the mechanical properties of an epoxy reinforced with boron carbide, J. Adhes. Sci. Technol. 25 (2011) 2445–2460.
[22] Q.X. Le, J.L. Torero, V.T.N. Dao, Understanding the effects of stress on the coefficient of thermal expansion, Int. J. Eng. Sci. 141 (2019) 83–94.
[23] O. Matvienko, O. Daneyko, T. Kovalevskaya, A. Khrustalyov, I. Zhukov, A. Vorozhtsov, Investigation of stresses induced due to the mismatch of the coefficients of thermal expansion of the matrix and the strengthening particle in aluminum-based composites, Metals (Basel) 11 (2021) 279.
[24] H. Yan, P. Wang, R. Li, Z. Xu, Aging behaviour of encapsulated assemblies of epoxy resin under accelerated thermal cycling, Int. J. Polym. Anal. Charact. 27 (2022) 180–194.
[25] N.L. Hancox, Thermal effects on polymer matrix composites: part 1.Thermal cycling, Mater. Des. 19 (1998) 85–91.
[26] S. Morsch, S. Lyon, P. Greensmith, S.D. Smith, S.R. Gibbon, Water transport in an epoxy–phenolic coating, Prog. Org. Coat. 78 (2015) 293–299.
[27] M.G. González, J.C. Cabanelas, J. Baselga, Applications of FTIR on epoxy resins-identification, monitoring the curing process, phase separation and water uptake, Infrared Spectrosc. Sci.Eng. Technol. 2 (2012) 261–284.
[28] C.A. Ramírez-Herrera, I. Cruz-Cruz, I.H. Jiménez-Cedeño, O. Martínez-Romero, A. Elías-Zúñiga, Influence of the epoxy resin process parameters on the mechanical properties of produced bidirectional [± 45°] carbon/epoxy woven composites, Polymers 13 (2021) 1273.
[29] N. Rajagopalan, A.S. Khanna, Effect of methyltrimethoxy silane modification on yellowing of epoxy coating on UV (B) exposure, J. Coat. 2014 (2014).
[30] A. Ghasemi-Kahrizsangi, J. Neshati, H. Shariatpanahi, E. Akbarinezhad, Improving the UV degradation resistance of epoxy coatings using modified carbon black nanoparticles, Prog. Org. Coat. 85 (2015) 199–207.
[31] B.K. Deka, T.K. Maji, Effect of TiO2 and nanoclay on the properties of wood polymer nanocomposite, Compos. Part A Appl. Sci. Manuf. 42 (2011) 2117–2125.
[32] A. Khalyavina, L. Häußler, A. Lederer, Effect of the degree of branching on the glass transition temperature of polyesters, Polymer 53 (2012) 1049–1053.
[33] K. Dusek, M. Duskova-Smrckova, Network structure formation during crosslinking of organic coating systems, Prog. Polym. Sci. 25 (2000) 1215–1260.
[34] A. Miszczyk, K. Darowicki, Water uptake in protective organic coatings and its reflection in measured coating impedance, Prog. Org. Coat. 124 (2018) 296–302.
[35] M. Jalili, M. Rostami, B. Ramezanzadeh, An investigation of the electrochemical action of the epoxy zinc-rich coatings containing surface modified aluminum nanoparticle, Appl. Surf. Sci. 328 (2015) 95–108.
[36] M. Musiani, M.E. Orazem, N. Pébère, B. Tribollet, V. Vivier, Determination of resistivity profiles in anti-corrosion coatings from constant-phase-element parameters, Prog. Org. Coat. 77 (2014) 2076–2083.